

Weak antilocalization in HgTe quantum well with inverted energy spectrum

G. M. Minkov,^{1,2} A. V. Germanenko,² O. E. Rut,² A. A. Sherstobitov,^{1,2} S. A. Dvoretzki,³ and N. N. Mikhailov³

¹*Institute of Metal Physics RAS, 620990 Ekaterinburg, Russia*

²*Institute of Natural Sciences, Ural Federal University, 620000 Ekaterinburg, Russia*

³*Institute of Semiconductor Physics RAS, 630090 Novosibirsk, Russia*

(Dated: February 7, 2012)

The results of experimental study of the magnetoconductivity of 2D electron gas caused by suppression of the interference quantum correction in HgTe single quantum well heterostructure with the inverted energy spectrum are presented. It is shown that only the antilocalization magnetoconductivity is observed at the relatively high conductivity $\sigma > (20 - 30) G_0$, where $G_0 = e^2/2\pi^2\hbar$. The antilocalization correction demonstrates a crossover from $0.5 \ln(\tau_\phi/\tau)$ to $1.0 \ln(\tau_\phi/\tau)$ behavior with the increasing conductivity or decreasing temperature (here τ_ϕ and τ are the phase relaxation and transport relaxation times, respectively). It is interpreted as a result of crossover to the regime when the two chiral branches of the electron energy spectrum contribute to the weak antilocalization independently. At lower conductivity $\sigma < (20 - 30) G_0$, the magnetoconductivity behaves itself analogously to that in usual 2D systems with the fast spin relaxation: being negative in low magnetic field it becomes positive in higher one. We have found that the temperature dependences of the fitting parameter τ_ϕ corresponding to the phase relaxation time demonstrate reasonable behavior, close to $1/T$, over the whole conductivity range from $5 G_0$ up to $130 G_0$. However, the τ_ϕ value remains practically independent of the conductivity in distinction to the conventional 2D systems with the simple energy spectrum, in which τ_ϕ is enhanced with the conductivity.

I. INTRODUCTION

New type of two-dimensional (2D) systems, which energy spectrum is formed by the spin-orbit interaction has attracted considerable interest during the last decade. Just in these structures the Dirac-like spectrum is realized. This leads to appearance of new and modification of traditional dependences of kinetic phenomena on the magnetic field, temperature, carriers density, etc. The graphene,^{1,2} topological insulators such as $\text{Bi}_{1-x}\text{Sb}_x$, Bi_2Se_3 , Bi_2Te_3 ,^{3,4} quantum wells of gapless semiconductor HgTe^{5,6} belong to this type of the system. In the last-mentioned, the energy spectrum can be tuned by changing of the quantum well width (d) from inverted at $d > d_c$ nm to the normal one at $d < d_c$,⁵ where $d_c \simeq (6 - 7)$ nm for CdTe/HgTe/CdTe heterostructure⁷ is the critical thickness of the HgTe layer corresponding to the collapse of the energy gap (see Fig. 1). Namely in the vicinity of d_c the Dirac-like spectrum is realized. Much progress in the growth technology of $\text{Hg}_{1-x}\text{Cd}_x\text{Te}/\text{HgTe}$ heterostructures^{8,9} gives possibility to carry out the detailed studies of the transport phenomena in such a type of 2D systems. Large number of the papers was devoted to studies of high magnetic field transport,¹⁰⁻¹² quantum Hall effect,^{13,14} crossover from the electron to hole conductivity in the gated structures.^{15,16} At the same time, effects resulting from the quantum interference were investigated in the sole experimental¹⁷ and sole theoretical¹⁸ paper.

In this work, we present the results of experimental study of the interference quantum correction to the conductivity ($\delta\sigma$) in the HgTe single quantum well with the inverted energy spectrum. It is shown that only the antilocalization magnetoconductivity is observed at relatively high conductivity $\sigma > (20 - 30) G_0$, where $G_0 =$

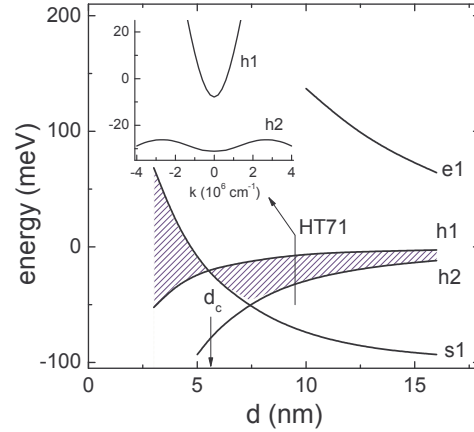


FIG. 1. (Color online) Energies of subbands at $k = 0$ as a function of the HgTe quantum well width for the $\text{Hg}_{0.35}\text{Cd}_{0.65}\text{Te}/\text{HgTe}/\text{Hg}_{0.35}\text{Cd}_{0.65}\text{Te}$ heterostructure calculated in the 6×6 \mathbf{kP} -model as described in Ref. 19 with parameters from Ref. 13. The dashed area indicates the energy gap. Inset shows the dispersion law for $d = 9.5$ nm corresponding to the structure HT71.

$e^2/2\pi^2\hbar$. It has been found that the antilocalization correction demonstrates a crossover from the regime when $\delta\sigma = -\alpha \ln(\tau_\phi/\tau)$ with $\alpha = -0.5$ to that with $\alpha = -1.0$ (τ_ϕ and τ are the phase relaxation and transport relaxation times, respectively). It is interpreted as a crossover to the regime when the two chiral branches of the energy spectrum contribute to the weak antilocalization independently. At lower conductivity $\sigma < (20 - 30) G_0$, the magnetoconductivity behaves itself analogously to that in usual 2D systems with the fast spin relaxation. The magnetoconductivity curves in this case are well fitted

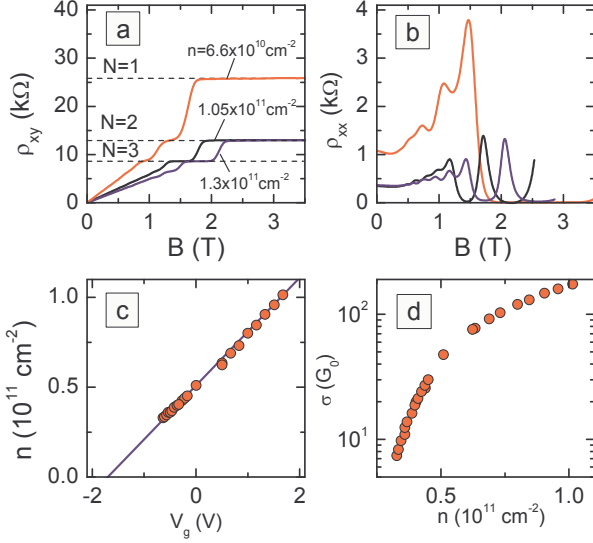


FIG. 2. (Color online) (a) and (b) – The magnetic field dependences of ρ_{xy} and ρ_{xx} , respectively, measured at $T = 1.35$ K for the different electron densities. (c) – The gate voltage dependences of the electron densities found as $n = -1/eR_H(0.1\text{ T})$, where R_H is the Hall coefficient, and the electron density dependence of the conductivity at $T = 1.35$ K are plotted in Fig. 2(c) and Fig. 2(d), respectively. As seen n vs V_g plot is close to the linear one and its slope corresponds to the geometric capacity $C = 4.8\text{ nF/cm}^2$ measured experimentally. (d) – The conductivity measured at $B = 0$ and $T = 1.35$ K as a function of the electron density.

by the standard expression.^{20,21} We find that the temperature dependences of τ_ϕ , which value is found from the fit, is close to $1/T$ law over the conductivity range $\sigma = (5 - 130)G_0$ as it should be when the inelasticity of electron-electron (e - e) interaction is the main mechanism of the phase relaxation.²² At the same time, the τ_ϕ value remains practically independent of the conductivity in contrast to the ordinary 2D systems, where τ_ϕ is roughly proportional to the conductivity.

II. EXPERIMENTAL

Our HgTe quantum wells were realized on the basis of HgTe/Hg_{1-x}Cd_xTe ($x = 0.5 - 0.65$) heterostructure grown by means of MBE on GaAs substrate with the (013) surface orientation.⁹ The three heterostructures HT108, HT71, and H922 with the nominal width of the quantum well equal to 9.0 nm, 9.5 nm, and 10 nm, respectively, were investigated. The samples were mesa etched into standard Hall bars. To change and control the electron density (n) in the quantum well, the field-effect transistors was fabricated on the basis of the Hall bars with parylene as an insulator and aluminium as gate electrode. In some cases the illumination was used to change the electron density in the quantum well. The conductivity of the structure HT71 after the cooling down to the liquid helium temperature was very low, $\sigma \simeq 10^{-2}G_0$, and enhanced up to $\simeq 130G_0$ with the help of illumination or application of the gate

voltage. The electron density in the structures HT108 and H922 at $V_g = 0$ was about $4.5 \times 10^{11}\text{ cm}^{-2}$ and $5.0 \times 10^{11}\text{ cm}^{-2}$, respectively, and decreased down to $(3 - 5) \times 10^{10}\text{ cm}^{-2}$ by the gate voltage. The electron mobility at $n = 1.0 \times 10^{11}\text{ cm}^{-2}$ was $1.3 \times 10^5\text{ cm}^2/\text{Vs}$, $4.5 \times 10^4\text{ cm}^2/\text{Vs}$, and $4.5 \times 10^4\text{ cm}^2/\text{Vs}$ in the structures HT71, HT108, and H922, respectively. The main results were analogous for all the structures. For this reason, the figures will represent the results obtained on the structure HT71, except as otherwise noted.

III. RESULTS AND DISCUSSION

The magnetic field dependences of off-diagonal and diagonal component of the resistivity tensor (ρ_{xy} and ρ_{xx}) at some gate voltages are presented in Fig. 2(a) and Fig. 2(b), respectively. Well-resolved quantum Hall plateaus, both the even and odd, are evident. The V_g dependence of the electron density found as $n = -1/eR_H(0.1\text{ T})$, where R_H is the Hall coefficient, and the electron density dependence of the conductivity at $T = 1.35$ K are plotted in Fig. 2(c) and Fig. 2(d), respectively. As seen n vs V_g plot is close to the linear one and its slope corresponds to the geometric capacity $C = 4.8\text{ nF/cm}^2$ measured on the same sample.

Let us consider the low field magnetoconductivity presented in Fig. 3. To compare the experimental curves measured at different conductivity values, we plot them against the relative magnetic field $b = B/B_{tr}$, where $B_{tr} = \hbar/2el^2$ with l as the mean free path is the characteristic magnetic field for the interference correction. Furthermore, we shift the experimental dependences $\Delta\sigma(b) = 1/\rho_{xx}(b) - 1/\rho_{xx}(0)$ in the vertical direction on the value of the interference correction at $B = 0$, $\delta\sigma(0)$, found as described in Section III C. So, the plotted in Fig. 3 dependence is actually the b dependence of the interference correction $\delta\sigma(b)$. One can see that only

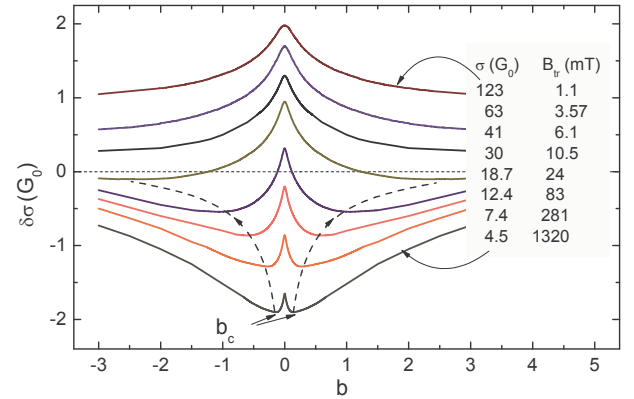


FIG. 3. (Color online) The dependences $\delta\sigma(b) = \Delta\sigma(b) + \delta\sigma(0)$ for different conductivity values, $T = 1.35$ K. The dashed arrows show the shift of the minimum with the increasing conductivity.

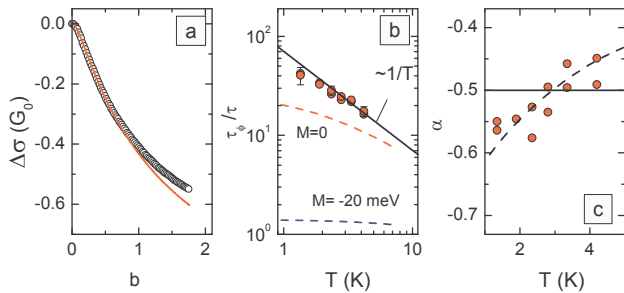


FIG. 4. (Color online) (a) – The magnetic field dependence of $\Delta\sigma$ for $n = 5.8 \times 10^{10} \text{ cm}^{-2}$, $\sigma = 63 G_0$, $T = 1.35 \text{ K}$. Symbols are the data, the curve is the results of the best fit by Eq. (2) carried out within the b range from 0 to 0.3. (b) – The temperature dependence of the phase relaxation time found from the fit of the magnetoconductivity curves. The symbols are the data. The dashed curves are calculated as described in Section III A. (c) – The temperature dependence of the prefactor α . The symbols are the data found from the fit, the dashed line is provided as a guide to the eye, the solid line is $\alpha = -0.5$.

the negative (antilocalizing) magnetoconductivity is observed at high conductivity $\sigma > (20 - 30) G_0$ over the whole magnetic field range up to $b = 3$. At lower conductivity values, the crossover to the positive magnetoconductivity is observed at the magnetic field labeled as b_c . As clearly seen from the figure the lower the conductivity the lower the value of b_c . At $\sigma < 20 G_0$ the value of b_c becomes less than unity.

A. Low-field positive magnetoconductivity, high conductivity $\sigma > 20 G_0$

So far as we know the theory of the interference induced magnetoconductivity for systems with complicated energy spectrum like HgTe quantum wells is not developed yet. Therefore, our analysis will lean upon the following qualitative consideration. As shown in Ref. 5 the HgTe quantum wells have a single-valley Dirac-like energy spectrum in the vicinity of the critical thickness d_c . It consists of two branches of different chirality (in what follows referred as k^+ and k^-), which are degenerate in a symmetric quantum well or can be split-off due to spin-orbit interaction in asymmetric case. The chiral fermions cannot be backscattered and the magnetoconductivity in such a type of heterostructures should demonstrate the antilocalization behavior. The contribution to the interference correction coming from each branch is positive and is equal to $0.5 G_0 \ln(\tau_\phi/\tau)$, $\tau_\phi \gg \tau$. When the transition rate $1/\tau_\pm$ between the branches k^+ and k^- is small as compared with the phase relaxation rate $1/\tau_\phi$, the interference contributions to the conductivity from these branches are summarized and the total correction should be equal to $(0.5 + 0.5) G_0 \ln(\tau_\phi/\tau)$. In opposite case, when $1/\tau_\pm \gg 1/\tau_\phi$, the correction should be equal to $0.5 G_0 \ln(\tau_\phi/\tau)$. So, the interference correc-

tion at $B = 0$ for arbitrary relationship between τ_ϕ and τ_\pm should be equal to

$$\delta\sigma = -\alpha G_0 \ln\left(\frac{\tau_\phi}{\tau}\right), \quad -1 \leq \alpha \leq -0.5. \quad (1)$$

The magnetoconductivity resulting from the suppression of the electron interference by the magnetic field should be described by the standard expression^{20,21} with same prefactor α :

$$\Delta\sigma(b) = \alpha G_0 \mathcal{H}\left(\frac{\tau}{\tau_\phi}, b\right),$$

$$\mathcal{H}(x, y) = \psi\left(\frac{1}{2} + \frac{x}{y}\right) - \psi\left(\frac{1}{2} + \frac{1}{y}\right) - \ln x, \quad (2)$$

where $\psi(x)$ is the digamma function. This equation with two fitting parameters α and τ_ϕ has been used for the quantitative analysis of our magnetoconductivity curves.²³ Because Eq. (2) is correct for the diffusion regime, i.e., for $b \ll 1$, the fitting range was restricted by the interval $0 < b < 0.3$. As an example, the result of the fitting procedure made for $\sigma = 63 G_0$ is presented in Fig. 4(a). One can see that Eq. (2) well describes the run of experimental curve.

The temperature dependences of the fitting parameter τ_ϕ/τ as Fig. 4(b) shows is close to $1/T$ law that corresponds to the inelasticity of e - e interaction as the main mechanism of the phase relaxation.²² Such the temperature dependence of τ_ϕ is observed over the entire conductivity range $20 G_0 < \sigma < 130 G_0$.

Let us call our attention to the prefactor, which temperature dependence is presented in Fig. 4(c). It is seen that the value of α is close to -0.5 and it becomes more negative with the decreasing temperature. The first-mentioned is indication of that the inter-branch transition time τ_\pm is comparable with or less than τ_ϕ . The fact that $|\alpha|$ is somewhat less than 0.5 at $T = 4.2 \text{ K}$ can be explained by not rigorous fulfilment of the condition $\tau_\phi \gg \tau$ under which Eq. (2) works. When this strong inequality is violated, our fitting procedure gives the value of τ_ϕ close to the true one, whereas α occurs to be reduced in magnitude.²⁴ For the case presented in Fig. 4, the ratio τ_ϕ/τ is about 15 – 20 at $T = 4.2 \text{ K}$ that should results in reduction of α by a factor of about 0.7. The increase of $|\alpha|$ observed with the T decrease may result from enhancement of τ_ϕ to τ_\pm ratio due to increase of the phase relaxation time with the decreasing temperature. This fact together with that α becomes appreciably less than -0.5 indicates that the system crosses over to the regime of independent contributions of each chiral branch to the interference correction.

Thus, the temperature dependences of both fitting parameters α and τ_ϕ are sound.

We turn now to the conductivity dependence of τ_ϕ and α shown in Fig. 5. The surprising thing is that the parameter τ_ϕ does not increase with the increasing conductivity as predicted theoretically²⁵ for the inelasticity of the e - e interaction as the main mechanism of the phase

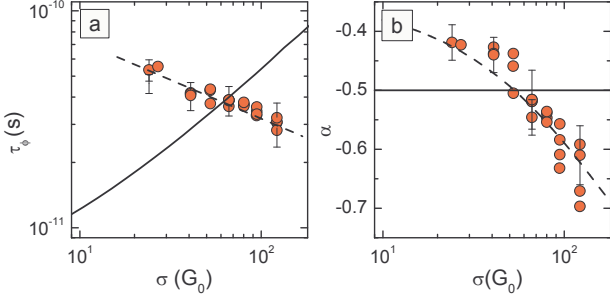


FIG. 5. (Color online) (a) – The values of τ_ϕ (a) and α (b) plotted against the conductivity at $T = 1.35$ K. The symbols are the data. The dashed lines are provided as a guide to the eye. The solid line in panel (a) is calculated in accordance with Ref. 25.

relaxation [see solid curve in Fig. 5(a)]. It should be also noted that the value of τ_ϕ found from the fit in HgTe quantum well at $\sigma \simeq 20 G_0$ is approximately 2.5–3 times as large as the theoretical value of the dephasing time. As Fig. 5(b) demonstrates the prefactor α increases in magnitude with the increasing conductivity. As discussed above such the behavior indicates that the inter-branch transition time τ_\pm becomes larger than the dephasing time τ_ϕ , and the 2D gas approaches the regime of the two independent contributions of k^+ and k^- states to the interference quantum correction.

To the best of our knowledge there is the sole theoretical paper¹⁸ where the interference correction to the conductivity in HgTe quantum well was studied. According to this paper the value of the correction at $B = 0$ is

$$\delta\sigma = -2\beta G_0 \ln \frac{\tau^{-1}}{\tau_M^{-1} + \tau_\phi^{-1}}, \quad (3)$$

$$\tau_M^{-1} = \frac{2}{\tau} \frac{(\mathcal{M} + \mathcal{B}k_F^2)^2}{\mathcal{A}^2 k_F^2 + (\mathcal{M} + \mathcal{B}k_F^2)^2}, \quad k_F = \sqrt{2\pi n}, \quad (4)$$

where \mathcal{M} is the band gap at the Dirac point, \mathcal{A} and \mathcal{B} are the band parameters responsible for the linear and quadratic parts of the energy spectrum, respectively,⁵ and $\beta > -1/2$ is the prefactor, which value depends on τ/τ_ϕ and τ/τ_M so that $\beta \simeq -1/2$ when $\tau/\tau_\phi, \tau/\tau_M \ll 1$ [see Eq. (53) in Ref. 18]. Equation (3) is structurally very similar to the conventional expression, Eq. (1), $1/\tau_\phi + 1/\tau_M$ stands instead of $1/\tau_\phi$ only. It is natural to suppose that the magnetoconductivity could be described by Eq. (2) with the same substitution. Under this assumption the fit of the data by Eq. (2) should give $1/\tau_\phi + 1/\tau_M$ instead of $1/\tau_\phi$. However, following this line of attack we are not able to interpret our results. To demonstrate this, we have depicted the temperature dependences of $\tau/(1/\tau_\phi + 1/\tau_M)$ calculated for the two \mathcal{M} values, $\mathcal{M} = 0$ and -20 meV, in Fig. 4(b). The parameters \mathcal{A} and \mathcal{B} were equal to 380 meV·nm and 850 meV·nm², respectively, in accordance with Ref. 6, and τ/τ_ϕ varied with the temperature as $\tau/\tau_\phi = 0.014 T$. One can see that contrary to what observed experi-

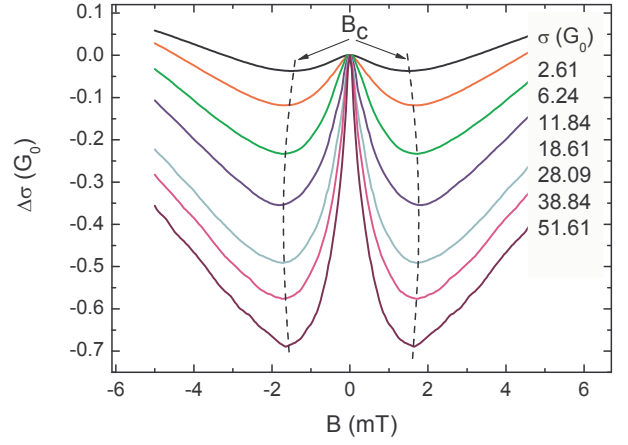


FIG. 6. (Color online) The magnetoconductivity plotted against the magnetic field for different σ at $T = 1.35$ K. The dashed lines demonstrate that the minimum position is practically independent of the conductivity.

mentally, the calculated dependences demonstrate very strong saturation with the temperature decrease, the saturation is more pronounced for $\mathcal{M} = -20$ meV, which is more appropriate to the structure investigated.

B. Alternative sign magnetoconductivity, $\sigma < 20 G_0$

Let us analyze the experimental results for the lower conductivity, $\sigma \lesssim 20 G_0$. In this case, the crossover from the negative magnetoconductivity to the positive one is observed at the magnetic field, which value is lower than the transport magnetic field, $b_c = B_c/B_{tr} \lesssim 1$ (see Fig. 3). At first sight $\Delta\sigma(b)$ behaves much like the interference induced magnetoconductivity observed in conventional 2D systems with the fast spin relaxation (see, e.g., Ref. 26). However, the fact that the crossover field B_c is practically independent of the conductivity, $B_c = (15 - 20)$ mT, as clearly seen from Fig. 6, sets one thinking about other possible reasons responsible for the crossover from the negative to positive magnetoconductivity at $B = B_c$.

In principle, the positive magnetoconductivity can result from the contribution of the e - e interaction. It should depend on the magnetic field due to the Zeeman splitting, which suppresses the interaction contribution in the triplet channel.^{27–33} If the value of the effective g -factor is sufficiently large, the Zeeman splitting $g\mu_B B$, where μ_B stands for the Bohr magneton, can exceed the temperature already in relatively low magnetic field, $B \sim 0.02$ T, and the positive magnetoconductivity resulting from this effect can win the negative magnetoconductivity caused by the quantum interference. Our measurements of the interaction correction with the use of the method suggested in Ref. 34 did not reveal any significant magnetic field dependence of the interaction correction in the actual magnetic-field range. However,

it must be admitted that the accuracy of this method at so low field is not very high to assert it unambiguously.

Another possible reason of the positive magnetoconductivity is classical memory effects.³⁵ As shown in Ref. 36, where the magnetotransport in the 2D Lorenz gas is studied, these effects due to double scattering of an electron on the same disk lead to a negative magnetoresistance even in classically weak magnetic field.^{36,37} However, our estimations made according to Ref. 37 with the use of typical for our case parameters show that the positive magnetoconductivity due to the memory effect is more than one order of magnitude less than the rise of the magnetoconductivity observed experimentally at $B > B_c$.

So, the known mechanisms of positive magnetoconductivity cannot explain our data. Therefore, despite the fact that the theory does not predict alternative sign magnetoconductivity for systems with the Dirac-like energy spectrum, let us analyze the data at $\sigma < 20 G_0$ under assumption that both rising and ascending parts

of the magnetoconductivity curves in Fig. 3 and Fig. 6 result from suppression of the interference correction in the magnetic field. In what follows, we will compare the shape of the magnetoconductivity curve with the well-known expressions employing the standard fitting procedure.

For the case when the spin-orbit splitting of the energy spectrum is cubic in quasimomentum the magnetoconductivity is described by the Hikami-Larkin-Nagaoka expression²⁰

$$\begin{aligned} \frac{\Delta\sigma(b)}{G_0} = & \psi\left(\frac{1}{2} + \frac{\tau}{b}\left[\frac{1}{\tau_\phi} + \frac{1}{\tau_s}\right]\right) - \ln\left(\frac{\tau}{b}\left[\frac{1}{\tau_\phi} + \frac{1}{\tau_s}\right]\right) \\ & + \frac{1}{2}\psi\left(\frac{1}{2} + \frac{\tau}{b}\left[\frac{1}{\tau_\phi} + \frac{2}{\tau_s}\right]\right) - \frac{1}{2}\ln\left(\frac{\tau}{b}\left[\frac{1}{\tau_\phi} + \frac{2}{\tau_s}\right]\right) \\ & - \frac{1}{2}\psi\left(\frac{1}{2} + \frac{\tau}{b}\frac{1}{\tau_\phi}\right) + \frac{1}{2}\ln\left(\frac{\tau}{b}\frac{1}{\tau_\phi}\right). \end{aligned} \quad (5)$$

Another case is the linear in quasimomentum splitting of the energy spectrum. According to Ref. 38 (see also comments in Ref. 39) $\Delta\sigma(b)$ in this case has the form

$$\begin{aligned} \frac{\Delta\sigma(b)}{G_0} = & \frac{1}{2} \left[\sum_{n=1}^{\infty} \left\{ \frac{3}{n} - \frac{3a_n^2 + 2a_nb_s - 1 - 2(2n+1)b_s}{(a_n + b_s)a_{n-1}a_{n+1} - 2b_s[(2n+1)a_n - 1]} \right\} - \frac{1}{a_0} - \frac{2a_0 + 1 + b_s}{a_1(a_0 + b_s) - 2b_s} \right. \\ & \left. - 2\ln(b_\phi + b_s) - \ln(b_\phi + 2b_s) - 3C - S(b_\phi/b_s) - \Psi(1/2 + b_\phi) + \ln b_\phi \right], \end{aligned} \quad (6)$$

where $C \approx 0.57721$ is the Euler constant, $b_\phi = b\tau/\tau_\phi$, $b_s = b\tau/\tau_s$, $a_n = n + 1/2 + b_\phi + b_s$, and $S(b_\phi/b_s)$ is the b -independent function

$$S(x) = \frac{8}{\sqrt{7+16x}} \left[\arctan \frac{\sqrt{7+16x}}{1-2x} - \pi\Theta(1-2x) \right]$$

with $\Theta(y)$ as the Heaviside step function. Expressions (5) and (6) have been derived under assumption that the conductivity is very high, $\sigma \gg G_0$. When it is not the case, one should regard for the second order quantum corrections. To take them into account we have multiplied the right-hand side of both expressions, Eq. (5) and Eq. (6), by the factor $1 - 2G_0/\sigma$ as it has been done for the case of slow spin relaxation in Ref. 40.

In Fig. 7(a), we demonstrate the results of the fitting procedure for $\sigma = 9.75 G_0$ carried out within the magnetic field range $b = 0 - 0.3$ with the use of τ_ϕ and τ_s as the fitting parameters. It is clearly seen that Eq. (6) does not describe the experimental data, while Eq. (5) gives very good agreement. Such the agreement is observed at all the temperatures from 1.3 K to 4.2 K over the conductivity interval from $5 G_0$ to $25 G_0$. Therewith, the temperature dependences of the fitting parameters τ_ϕ and τ_s corresponding to the phase and spin relaxation times, respectively, are reasonable. Again, τ_ϕ demonstrates behavior close to $1/T$ law, while τ_s is temperature independent within our accuracy [see Fig. 7(b)] that

is typical for the degenerate gas of carriers.

C. Overview of entire conductivity range, $\sigma = (5 - 130) G_0$

Let us now inspect how the results obtained within the different conductivity ranges dovetail into one another. The τ_ϕ values found for different conductivity regions as described above are graphed as a function of the conductivity in Fig. 8(a). The values of the interference correction at $B = 0$ calculated from Eq. (1) at high conductivity, $\sigma > 20 G_0$, and from the expression

$$\frac{\delta\sigma(0)}{G_0} = -\frac{1}{2}\ln\frac{\tau}{\tau_\phi} + \ln\left(\frac{\tau}{\tau_\phi} + \frac{\tau}{\tau_s}\right) + \frac{1}{2}\ln\left(\frac{\tau}{\tau_\phi} + \frac{2\tau}{\tau_s}\right) \quad (7)$$

at lower one are plotted in Fig. 8(b). It is seen that both τ_ϕ vs σ and $\delta\sigma$ vs σ dependences found by the two different methods within the low- and high-conductivity regions are matched well near $\sigma \simeq 30 G_0$. Namely these values of $\delta\sigma(0)$ have been used to shift the experimental dependences $\Delta\sigma(b)$ in the vertical direction in Fig. 3. An essential feature evident from Fig. 8(a) is that the fitting parameter τ_ϕ does not practically depend on the conductivity over the whole conductivity range from $\sigma \simeq 5 G_0$ to $\sigma \simeq 130 G_0$. Such the behavior is in qualitative disagreement with that observed in conventional A_3B_5 -

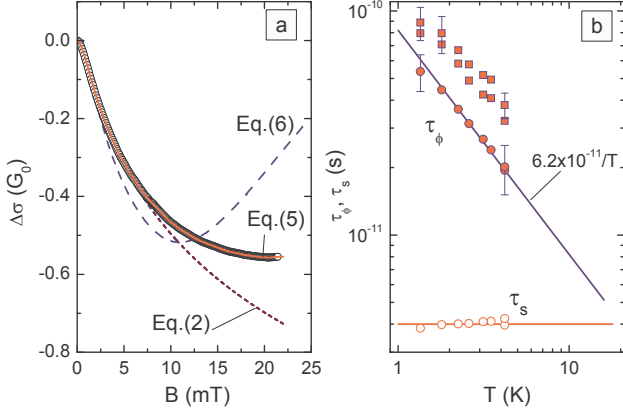


FIG. 7. (Color online) (a) – The magnetoconductivity plotted as a function of the magnetic field for $\sigma = 9.75 G_0$ ($B_{tr} = 62$ mT) at $T = 1.35$ K. The symbols are the data, the lines are the results of the fitting procedure by the different expressions. (b) – The temperature dependences of τ_ϕ and τ_s obtained with the help of Eq. (5) (circles) and Eq. (2) (squares).

based 2D electron systems. For instance, the dephasing time found experimentally in GaAs/In_{0.2}Ga_{0.8}As/GaAs single quantum well heterostructures increases about five times over the same conductivity range,⁴⁰ that accords well with the theoretical prediction²⁵ [see line and open squares in Fig. 8(a)].

As already mentioned above the crossover to the positive magnetoconductivity evident at B_c can result from other mechanisms, i.e., only the negative magnetoconductivity at $B < B_c$ is caused by suppression of the electron interference, while another unknown mechanism is responsible for the positive magnetoconductivity at $B > B_c$. Then, Eq. (2) rather than Eq. (5) should be used to obtain the value of τ_ϕ at low conductivity $\sigma < 20 G_0$ as it took place for $\sigma > 20 G_0$, and the fitting region should be restricted by the field lower than B_c . The result of such a data treatment for $\sigma = 9.75 G_0$ ($B_{tr} = 62$ mT) is presented in Fig. 7(a) by the dotted line. The fit with the use of τ_ϕ and α as the fitting parameters has been made within the magnetic field range $B = (0 - 1.5)$ mT. The prefactor α obtained from the fit is equal to -0.33 , which is close to that expected theoretically $\alpha \simeq -0.5(1 - 2G_0/\sigma) \simeq -0.4$. The temperature dependence of τ_ϕ is close to $1/T$, while the value of τ_ϕ is somewhat larger than that found with help of Eq.(5) [see Fig. 7(b)]. Analogous results are obtained within whole low-conductivity range down to $\sigma = 5 G_0$, but, what is more important, the use of Eq. (2) over the entire conductivity range gives just the same result: τ_ϕ does not increase with the increasing conductivity.

It is pertinent here to direct the reader's attention to the results obtained on the topological insulator Bi₂Se₃ and reported recently in Ref. 41. The authors present the gate voltage dependence of $B_\phi = \hbar/4eD\tau_\phi$ (D is the diffusion coefficient) found from the fit of the experimental

magnetoconductivity curves by Eq. (2). It is possible for some V_g values to convert these data to τ_ϕ vs σ dependence. To do this one should know the dependence of the effective mass (m) on the electron density. If one believes that m is constant in respect to n , we obtain that τ_ϕ in Bi₂Se₃ decreases with the increasing conductivity within the range $\sigma = (50 - 500) G_0$. However, if one naturally supposes that $m \propto \sqrt{n}$, that corresponds to the linear Dirac-like spectrum, we obtain result analogous to that presented above for HgTe quantum well: τ_ϕ is practically independent of σ .

Before closing this section let us list possible reasons for so different behavior of τ_ϕ with changing σ in the 2D systems with conventional parabolic energy spectrum and in the systems with complicated spectrum like HgTe single quantum wells. First, the parameters τ_ϕ and τ_s found from the fit may not correspond to the true phase and spin relaxation times despite the fact that the standard expressions, Eq. (2) and Eq. (5), fit the experimental magnetoconductivity curves rather well. Another expression, which properly takes into account the peculiarities of the energy spectrum and electron interference in the HgTe 2D systems should be derived and used. Second, τ_ϕ found from the fit is true or close to that, but inelasticity of the e - e interaction in the systems with complicated energy spectrum depends on the conductivity really much weaker than in the conventional systems or there is more effective additional mechanism of inelastic phase relaxation in the structures under study that changes the dependence $\tau_\phi(\sigma)$ drastically. However, it remains unclear in the last case why the dephasing time at low conductivity is five-to-ten times larger in HgTe quantum well than

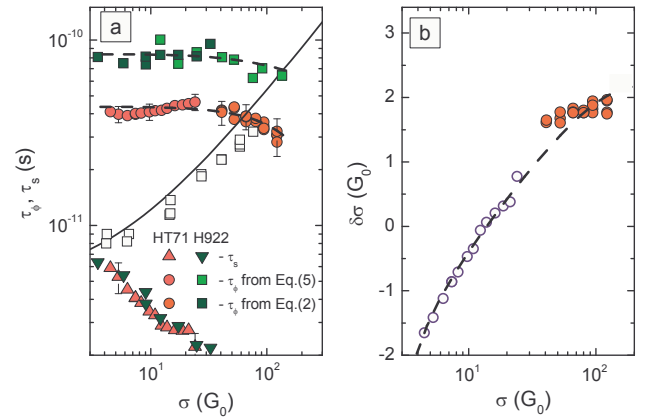


FIG. 8. (Color online) (a) – The values of τ_ϕ and τ_s plotted against the conductivity for $T = 1.35$ K for the structures HT71 and H922. The line is calculated according to Ref. 25. The open squares are the experimental results obtained in Ref. 40 on the sample H451 with GaAs/In_{0.2}Ga_{0.8}As/GaAs quantum well. (b) – The value of interference correction at zero magnetic field found from Eq. (1) (solid circles) and Eq. (7) (open circles) as a function of the conductivity for $T = 1.35$ K, structure HT71. The dashed lines in both panels are provided as a guide to the eye.

that in conventional 2D systems as Fig. 8(a) illustrates.

IV. CONCLUSION

We have studied the interference induced magnetoconductivity in single quantum well of gapless semiconductor HgTe with the inverted energy spectrum. It is shown that only the antilocalization magnetoconductivity is observed at relatively high conductivity $\sigma > (20 - 30) G_0$. The antilocalization correction demonstrates the crossover from the $0.5 \ln(\tau_\phi/\tau)$ to $1.0 \ln(\tau_\phi/\tau)$ behavior with the increasing conductivity or decreasing temperature that is interpreted as a result of crossover to the regime of independent contributions of the two chiral branches to the weak antilocalization. At lower conductivity $\sigma < (20 - 30) G_0$, the magnetoconductivity behaves itself analogously to that in usual 2D systems with the

fast spin relaxation. It is negative in low magnetic field and becomes positive in higher one. We have found that the temperature dependences of the fitting parameters τ_ϕ corresponding to the phase relaxation times is close to $1/T$ over the whole conductivity range $\sigma = (5 - 130) G_0$ that is typical for the dirty 2D systems at low temperature. However, the τ_ϕ value is practically independent of the conductivity unlike the conventional 2D systems with the simple energy spectrum, in which τ_ϕ increases with the growing conductivity.

ACKNOWLEDGMENTS

We would like to thank I. V. Gornyi and I. S. Burmistrov for illuminating discussions. This work has been supported in part by the RFBR (Grant Nos. 10-02-91336 and 10-02-00481).

-
- ¹ A. K. Geim, Rev. Mod. Phys., **83**, 851 (2011).
 - ² K. S. Novoselov, Rev. Mod. Phys., **83**, 837 (2011).
 - ³ M. Z. Hasan and C. L. Kane, Rev. Mod. Phys., **82**, 3045 (2010).
 - ⁴ M. Z. Hasan, D. Hsieh, Y. Xia, L. A. Wray, S.-Y. Xu, and C. L. Kane, arXiv:1105.0396v1 [cond-mat.mes-hall].
 - ⁵ B. A. Bernevig, T. L. Hughes, and S.-C. Zhang, Science, **314**, 1757 (2006).
 - ⁶ B. Buttner, C. X. Liu, G. Tkachov, E. G. Novik, C. Brune, H. Buhmann, E. M. Hankiewicz, P. Recher, B. Trauzettel, S. C. Zhang, and L. W. Molenkamp, Nature Phys., **7**, 418 (2011).
 - ⁷ L. G. Gerchikov and A. Subashiev, Phys. Stat. Sol. (b), **160**, 443 (1990).
 - ⁸ F. Goschenhofer, J. Gerschutz, A. Pfeuffer-Jeschke, R. Hellmig, C. R. Becker, and G. Landwehr, J. Electron. Mater., **27**, 532 (1998).
 - ⁹ N. N. Mikhailov, R. N. Smirnov, S. A. Dvoretzky, Y. G. Sidorov, V. A. Shvets, E. V. Spesivtsev, and S. V. Rykhlitski, Int. J. Nanotechnology, **3**, 120 (2006).
 - ¹⁰ X. C. Zhang, A. Pfeuffer-Jeschke, K. Ortner, C. R. Becker, and G. Landwehr, Phys. Rev. B, **65**, 045324 (2002).
 - ¹¹ X. C. Zhang, K. Ortner, A. Pfeuffer-Jeschke, C. R. Becker, and G. Landwehr, Phys. Rev. B, **69**, 115340 (2004).
 - ¹² G. M. Gusev, Z. D. Kvon, O. A. Shegai, N. N. Mikhailov, S. A. Dvoretzky, and J. C. Portal, Phys. Rev. B, **84**, 121302 (2011).
 - ¹³ K. Ortner, X. C. Zhang, A. Pfeuffer-Jeschke, C. R. Becker, G. Landwehr, and L. W. Molenkamp, Phys. Rev. B, **66**, 075322 (2002).
 - ¹⁴ G. M. Gusev, E. B. Olshanetsky, Z. D. Kvon, N. N. Mikhailov, S. A. Dvoretzky, and J. C. Portal, Phys. Rev. Lett., **104**, 166401 (2010).
 - ¹⁵ M. König, S. Wiedmann, C. Brüne, A. Roth, H. Buhmann, L. W. Molenkamp, X.-L. Qi, and S.-C. Zhang, Science, **318**, 766 (2007).
 - ¹⁶ Z. D. Kvon, E. B. Olshanetsky, E. G. Novik, D. A. Kozlov, N. N. Mikhailov, I. O. Parm, and S. A. Dvoretzky, Phys. Rev. B, **83**, 193304 (2011).
 - ¹⁷ E. B. Olshanetsky, Z. D. Kvon, G. M. Gusev, N. N. Mikhailov, S. A. Dvoretzky, and J. C. Portal, JETP Lett., **91**, 347 (2010).
 - ¹⁸ G. Tkachov and E. M. Hankiewicz, Phys. Rev. B, **84**, 035444 (2011).
 - ¹⁹ V. A. Larionova and A. V. Germanenko, Phys. Rev. B, **55**, 13062 (1997).
 - ²⁰ S. Hikami, A. I. Larkin, and Y. Nagaoka, Prog. Theor. Phys., **63**, 707 (1980).
 - ²¹ H.-P. Wittmann and A. Schmid, J. Low Temp. Phys., **69**, 131 (1987).
 - ²² B. L. Altshuler and A. G. Aronov, in *Electron-Electron Interaction in Disordered Systems*, edited by A. L. Efros and M. Pollak (North Holland, Amsterdam, 1985) p. 1.
 - ²³ Treating the magnetoconductivity curves we have supposed that the electron effective mass is independent of the electron density and is equal to $0.022 m_0$, which has been obtained from the Shubnikov-de Haas experiments for $n = 8 \times 10^{10} \text{ cm}^{-2}$. Our calculations show that the variation of the effective mass does not exceed (10-15)% within the actual range of the electron density from $3 \times 10^{10} \text{ cm}^{-2}$ to $1.5 \times 10^{11} \text{ cm}^{-2}$.
 - ²⁴ G. M. Minkov, A. V. Germanenko, V. A. Larionova, S. A. Negashev, and I. V. Gornyi, Phys. Rev. B, **61**, 13164 (2000).
 - ²⁵ G. Zala, B. N. Narozhny, and I. L. Aleiner, Phys. Rev. B, **64**, 214204 (2001).
 - ²⁶ W. Knap, A. Zduniak, L. H. Dmowski, S. Contreras, and M. I. Dyakonov, Phys. Stat. Sol. (b), **198**, 267 (1996).
 - ²⁷ C. Castellani, C. Di Castro, P. A. Lee, M. Ma, S. Sorella, and E. Tabet, Phys. Rev. B, **30**, 1596 (1984).
 - ²⁸ A. M. Finkel'stein, Zh. Eksp. Teor. Fiz., **86**, 367 (1984), [Sov. Phys. JETP **59**, 212 (1984)].
 - ²⁹ R. Raimondi, C. Castellani, and C. Di Castro, Phys. Rev. B, **42**, 4724 (1990).
 - ³⁰ C. Castellani, C. Di Castro, and P. A. Lee, Phys. Rev. B, **57**, R9381 (1998).
 - ³¹ G. Zala, B. N. Narozhny, and I. L. Aleiner, Phys. Rev. B, **65**, 020201 (2001).

- ³² I. V. Gornyi and A. D. Mirlin, Phys. Rev. B, **69**, 045313 (2004).
- ³³ G. M. Minkov, A. A. Sherstobitov, A. V. Germanenko, O. E. Rut, V. A. Larionova, and B. N. Zvonkov, Phys. Rev. B, **72**, 165325 (2005).
- ³⁴ G. M. Minkov, O. E. Rut, A. V. Germanenko, A. A. Sherstobitov, V. I. Shashkin, O. I. Khrykin, and B. N. Zvonkov, Phys. Rev. B, **67**, 205306 (2003).
- ³⁵ E. M. Baskin, L. N. Magarill, and M. V. Entin, Sov. Phys. JETP, **48**, 365 (1978).
- ³⁶ A. Dmitriev, M. Dyakonov, and R. Jullien, Phys. Rev. B, **64**, 233321 (2001).
- ³⁷ V. V. Cheianov, A. P. Dmitriev, and V. Y. Kachorovskii, Phys. Rev. B, **70**, 245307 (2004).
- ³⁸ S. V. Iordanskii, Y. B. Lyanda-Geller, and G. E. Pikus., Zh. Eksp. Teor. Fiz., **60**, 199 (1994), [JETP Lett. 60, 206 (1994)].
- ³⁹ G. M. Minkov, A. V. Germanenko, O. E. Rut, A. A. Sherstobitov, L. E. Golub, B. N. Zvonkov, and M. Willander., Phys. Rev. B, **70**, 155323 (1 (2004).
- ⁴⁰ G. M. Minkov, A. V. Germanenko, and I. V. Gornyi, Phys. Rev. B, **70**, 245423 (2004).
- ⁴¹ A. T. Hatke, M. A. Zudov, L. N. Pfeiffer, and K. W. West, Phys. Rev. B, **84**, 241304 (2011).